Advances in Science and Technology Research Journal

Advances in Science and Technology Research Journal, 2025, 19(11), 149–161
https://doi.org/10.12913/22998624/208849
ISSN 2299-8624, License CC-BY 4.0

Received: 2025.06.02
Accepted: 2025.09.15
Published: 2025.10.01

The fatigue strength of thin-walled shell structures with cutouts, in post-critical deformation states

Przemysław Alfred Mazurek[1]

[1] Rzeszów University of Technology, The Faculty of Mechanical Engineering and Aeronautics, Al. Powstańców Warszawy 8, 35-959 Rzeszów, Poland
E-mail: pmazurek@prz.edu.pl

ABSTRACT

The study presents the results of research on thin-walled elements made of aluminum alloy, subjected to pure shear. These elements represent a representative section of the skin of a semi-monocoque aircraft structure, weakened by an inspection hole. The possibility of the occurrence of post-critical deformations under operational load conditions was considered. The results of a numerical analysis conducted under static load conditions using the finite element method are presented. Based on the obtained stress distribution, a fatigue strength simulation was performed, based on the ε-n analysis. The results were verified using experimental static and fatigue tests.

Keywords: numerical analysis, experimental tests, buckling, postbuckling.

INTRODUCTION

In most cases of structures, the issue of stability loss under operational conditions is limited to determining the value of the critical load. Based on this, geometric parameters of individual structural elements are defined to ensure that buckling does not occur in any area. In the early days of aviation development, this approach was also applied to aircraft components. The skin was given a sufficient thickness to prevent buckling. However, this led to a significant increase in weight. Other methods to increase the stiffness of skin elements included the use of corrugated or ribbed sheets; however, this resulted in increased aerodynamic drag, which in turn reduced cruising speed and increased fuel consumption.

With the development of aircraft structures and comprehensive experimental research, the acceptance of stability loss phenomena in skin panels has become common [1–5], albeit under certain conditions. The loss of stability in an aircraft's skin may only occur locally, meaning within a single panel, bounded by rigid structural elements (stringers, ribs, longerons), and should be elastic in nature [6–10]. The prevalence of post-critical deformation phenomena in aircraft skins arises from sufficient knowledge about the physical phenomena occurring in structures made of aluminum alloys, as well as an understanding of fatigue issues. However, various structural discontinuities in the form of cutouts (e.g., inspection windows and access holes) present additional challenges. Such areas, even if their dimensions are small compared to the size of the entire skin panel, pose a significant safety risk for aircraft operation. This is due to the change in the nature of stability loss compared to areas not containing these kinds of singularities, resulting in strong, localized stress concentrations.

Currently, computational numerical tools based on the finite element method [11] are widely used to address such issues. In the case of linear analyses, given the advancement of commercial software [12, 13], the results can generally be considered reliable. However, advanced deformation states and the resulting changes in the orientation of active force vectors require the application of nonlinear procedures. This introduces several challenges due to their limited reliability

when determining the equilibrium state of the structure during subsequent load increments. For this reason, experimental determination of the final deformation shape and the various stages leading to it is essential. Experimentally validated accuracy of numerical calculations serves as the basis for accepting the obtained stress distributions as reliable.

Knowledge of the stress distribution is crucial for the numerical prediction of fatigue strength. The use of commercial computational programs, such as MSC Fatigue [12], Fe-Safe [14], nCode [15], ANSYS [16], allows for the simulation of various operational conditions of the structure by generating multiple cases of variable load spectra within the software. However, the calculations are based on results obtained from static analysis and the generated material model, considered in terms of resistance to cyclic loads. The multitude of factors influencing the occurrence of fatigue damage can result in discrepancies between numerical simulation results and the actual durability of the structure under real-world conditions. Therefore, it is necessary to conduct experimental fatigue tests for at least the most representative case of the operational load spectrum.

THE SUBJECT AND SCOPE OF STUDY

The subject of the research presented in this work was thin-walled structures with cutouts, subjected to pure shear and operating in a state of post-critical deformation (Figure 1).

Such an element represents a fragment of the skin of an aircraft's load-bearing structure, bounded by ribs and stringers, with a small inspection hole present (Figure 2).

The small dimensions of such cutouts sometimes lead to a lack of careful analysis regarding their impact on the stiffness of the weakened element. In general, in mechanical structures, a static test is often sufficient, and a positive result permits the component to enter service. However, in the case of aircraft structures, such structural discontinuities can become a cause of fatigue crack formation.

The aim of the conducted research was to determine the influence of a small cutout on the form of post-critical deformation in comparison to an element without such discontinuities. The analyses were based on experimental studies conducted on two types of elements made of aluminum alloy. The deformation shape was assessed using an optical scanner. The results of these studies provided a basis for verifying the numerical models. Based on the obtained stress distributions, a numerical simulation of fatigue life was performed using the ε-n (strain – number of cycles) numerical analysis. The element with the cutout underwent

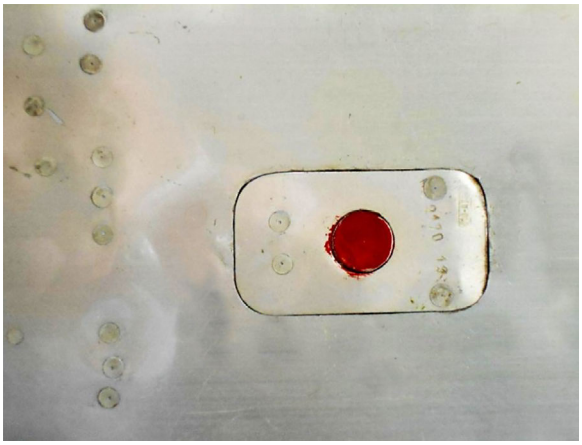

Figure 2. Example inspection hole with a cover

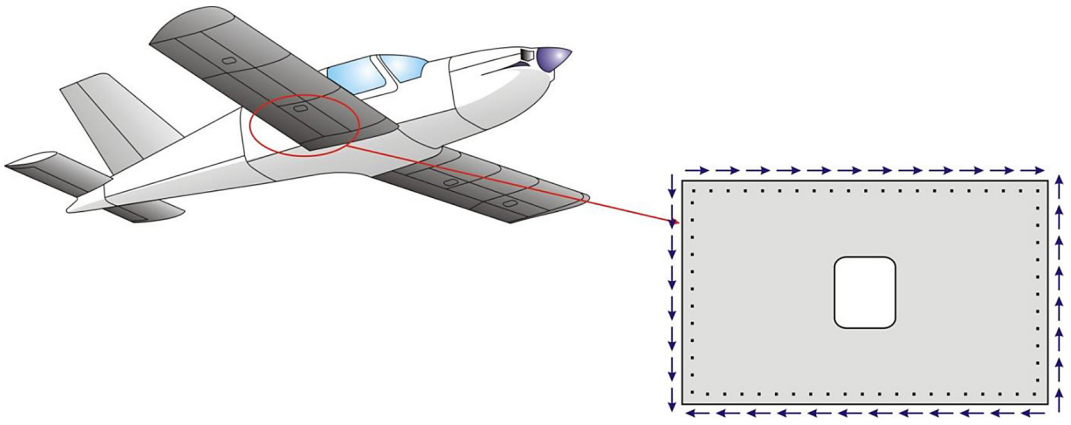

Figure 1. Example area of an aircraft structure with an inspection hole

experimental fatigue testing, allowing for the determination of the moment of crack initiation at a length of 2 mm (considered as the damage criterion according to the ε-n analysis), as well as the rate of growth of the fatigue crack.

STATIC EXPERIMENTAL STUDIES

The subject of the experiment consisted of thin-walled elements with a thickness of 0.6 mm, made from aluminum alloy designated 2024 (equivalent to PA7) [17, 18], subjected to pure shear. A cutout with dimensions of 35 × 35 mm, made in the second of the tested elements, had rounded corners, with the radius of curvature measuring 5 mm (Figure 3).

The elements were mounted in rigid steel edges made of T-cross beams of dimensions 40 × 40, with their corners connected jointedly, according to the predetermined loading scheme (Figure 4). This type of setup simulates a connection model similar to the interaction of the covering with rigid frame elements in an aircraft structure while

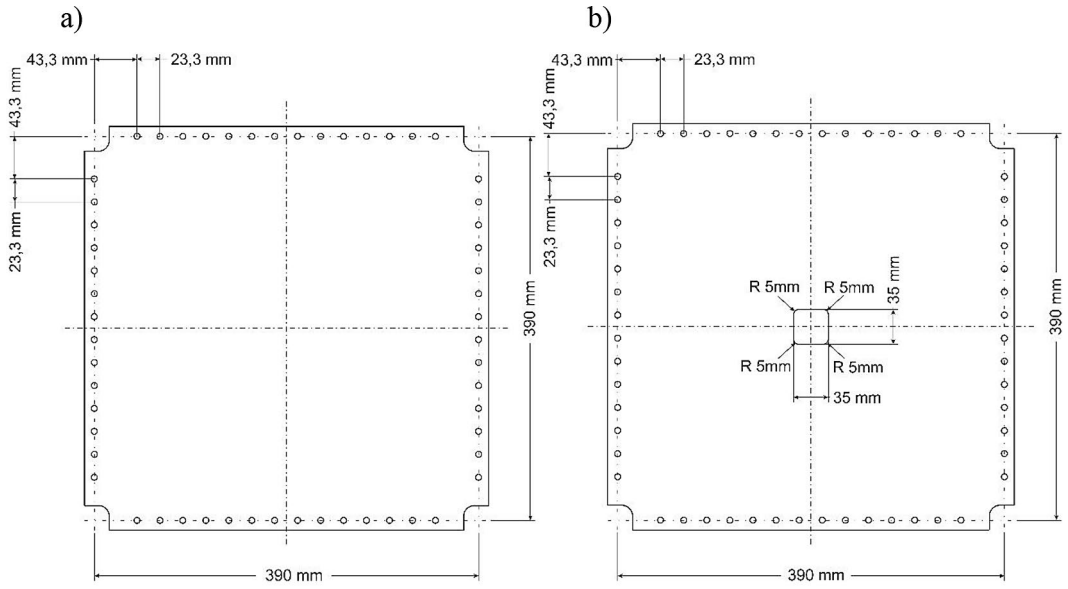

Figure 3. Geometry of the tested elements: (a) element without cutout, (b) element with cutout

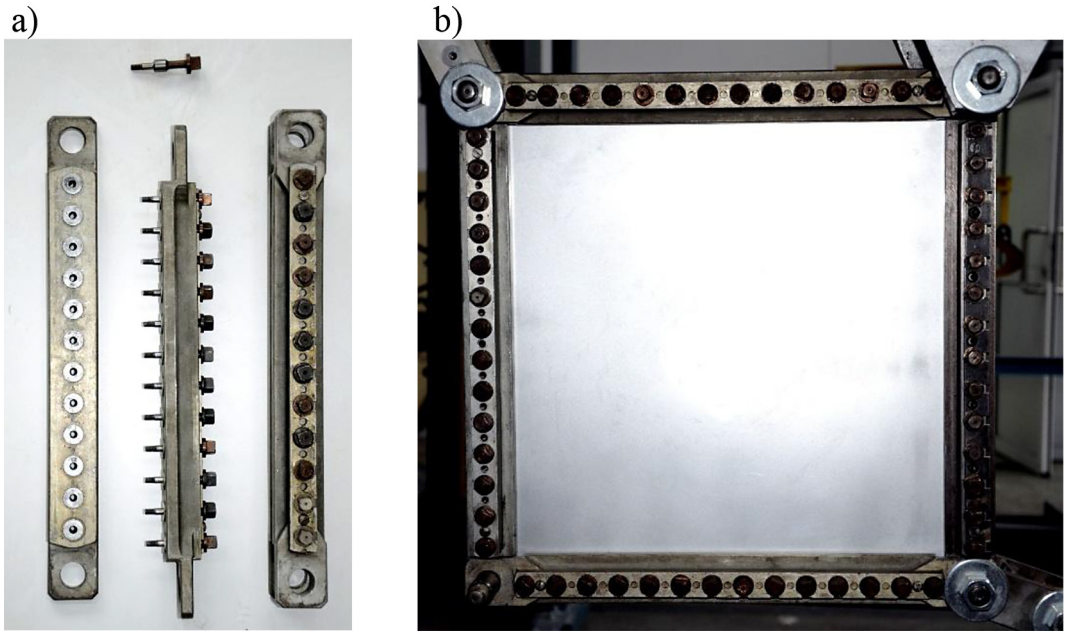

Figure 4. Rigid steel edges: (a) parts of edges, (b) The complete assembly, including the shell

applying loads in the form of pure shear. The assembled setup was fixed in a loading system powered by a single-sided lever, using a Zwick-Roell electromechanical actuator. Displacement measurements of reference points and the deformation field were carried out using a GOM Atos 3D scanner (Figure 5).

The deformation field of the deformed structure is presented in the form of maps of displacement. In both cases shown, a predominant fold is clearly visible along the diagonal of the element. Additionally, there are somewhat smaller folds that have formed on both sides (Figure 6).

In the case of the element with a cutout, there is a noticeable increase in the value of the normal displacement to the surface of the tested structure (by 33%) compared to the element without a cutout. Furthermore, the area occupied by the predominant fold is significantly narrower in the element with the cutout, resulting in the formation of a curvature with a smaller radius, which in turn leads to a substantial increase in the stress gradient due to the bending effect.

The primary criterion for assessing changes in the state of the structure as a function of the increase in load is the equilibrium path. Given that, for a multidimensional system, it is a hypersurface in the state hyperspace, which cannot be clearly represented in the form of a graph, it is generally assumed to take one representative parameter. In the considered case, the equilibrium paths were determined as the angle of deformation as a function of the load. The deformation angle measurement was conducted based on reference

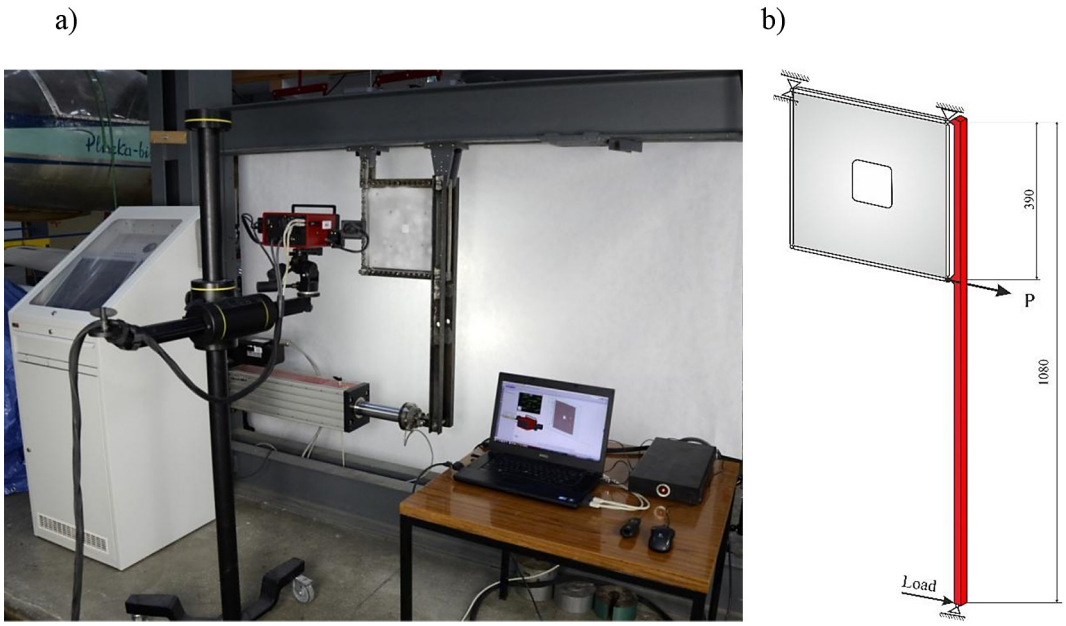

Figure 5. Measurement setup: (a) measurement station with the 3D Atos scanner, (b) loading system diagram

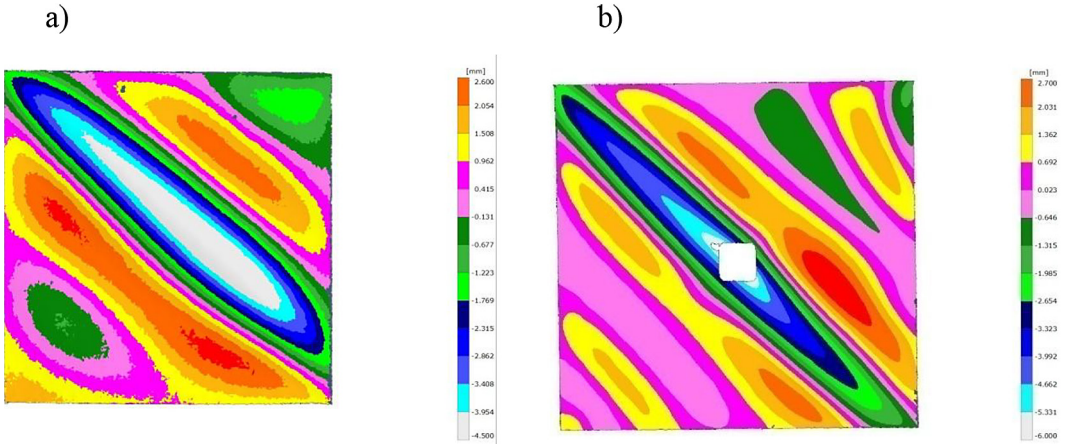

Figure 6. Normal deformation field of the structure: (a) element without a cutout, (b) element with a cutout

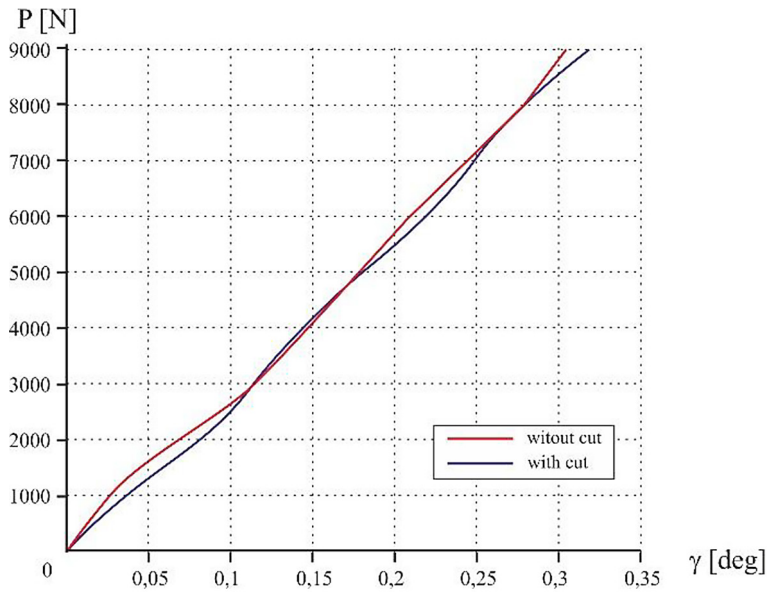

Figure 7. Representative equilibrium paths

points using a 3D scanner GOM-Atos.. The representative equilibrium paths for both versions of the tested elements, obtained from experimental studies, are presented below (Figure 7).

In the case of the element without a cutout, a slightly larger slope of the graph is noticeable in the initial loading phase, with a clearly observable point of loss of stability at a load of approximately Pkr = 1300 N. For the element with a cutout, the graph approximately maintains a constant slope, making it impossible to determine the critical load. In the range of loads between 3 kN and 5 kN, the graphs exhibit a similar trend, indicating the emergence of a stable form of deformation in both cases.

NONLINEAR NUMERICAL ANALYSIS

The information obtained from experimental research regarding the form of deformation allowed for the development of adequate numerical models and the performance of their nonlinear analysis [19, 20]. For the calculations, the MSC Patran/MARC [13] software was used, which operates based on the finite element method. The results of the numerical analyses were evaluated based on the criterion of satisfactory agreement of the deformation form and representative equilibrium paths compared to the results of experimental studies.

In both cases, surface models were used to model the investigated elements as well as the rigid edges. A fixed support was applied at the top-right corner of the frame, while a roller support was used at the top-left corner by releasing the horizontal degree of freedom. In the bottom corners, the degrees of freedom perpendicular to the plane of the structure were constrained. Below are the numerical models along with the boundary conditions and the applied load (Figure 8). Four-node elements with bilinear interpolation of shape functions, with six degrees of freedom per node were used. In the model without a cutout, the mesh consisted of approximately 5200 two-dimensional thin shell elements (global size of finite elements was 5 mm), while the element with a cutout was constructed using around 16600 thin shell elements (global size of finite elements was 5 mm, gradually reduced to 0.4mm in the corners). This was due to the need to accurately reproduce the corner area of the cutout, where strong stress gradients were expected. In both cases, approximately 2000 thick shell elements were used to model the rigid framing.

The analyzed structures were assigned a linearly elastic material model with parameters corresponding to aluminum alloy 2024, while for the rigid edges, material parameters corresponding to steel were used (Table 1).

Due to advanced post-buckling (post-critical) deformations, nonlinear analyses were conducted using the MSC Marc solver [13], employing the Newton-Raphson method [11, 19, 20]. The deformation values obtained from the numerical

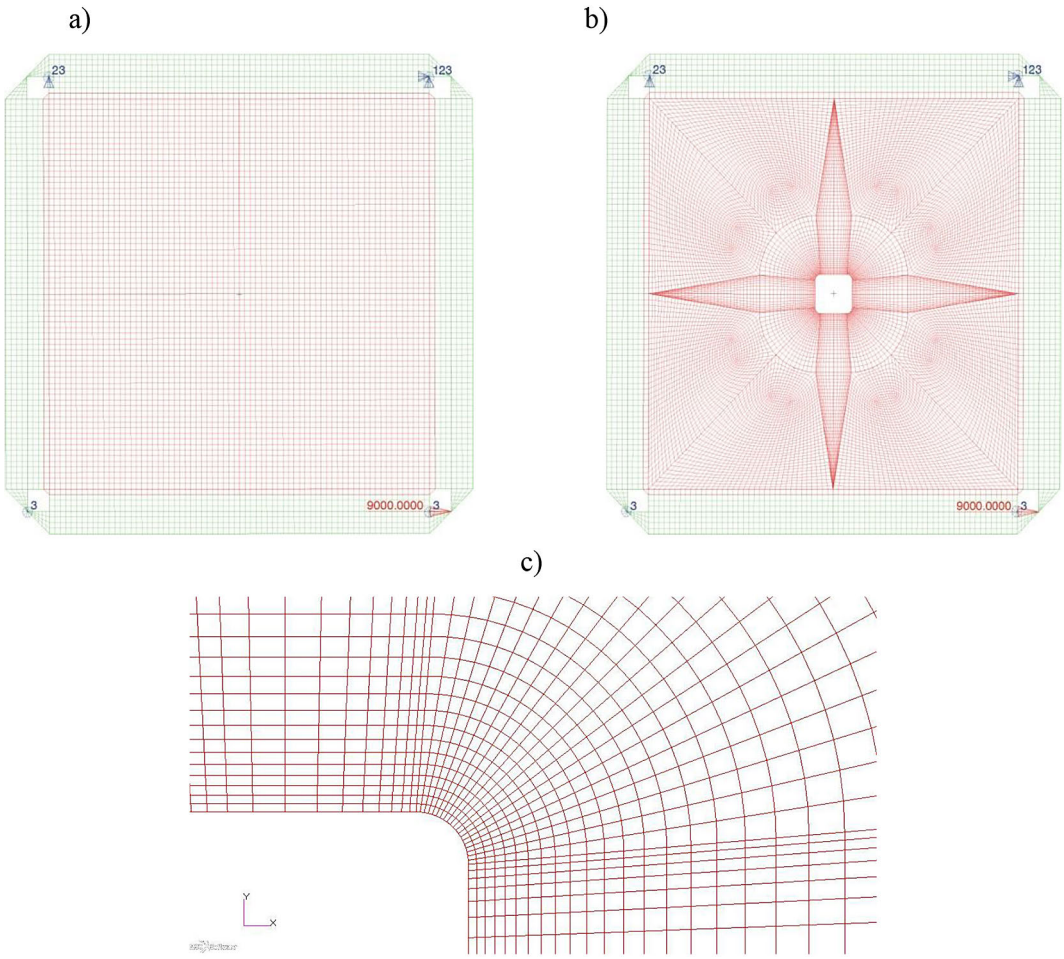

Figure 8. Finite element mesh: (a) model without a cutout, (b) model with a cutout, (c) details of mesh modeling in the corner of the cutout

Table 1. Quasi-static mechanical properties of materials

Parameter	E [MPa]	v	*UTS* [MPa]	*YS* [MPa]
Al 2024	7.4 · 10^4	0.34	470	372
Steel	2.1 · 10^5	0.3	1200	850

analyses are presented in the form maps of displacement (Figure 9).

The deformation fields obtained through numerical calculations correspond to analogous images obtained from experimental studies, both qualitatively and quantitatively. Some irregularities and small additional folds that appear during the experiment are caused by the initial deviations of the actual elements from the ideal geometry and assembly clearance in the corners of the rigid edges, allowing for transverse displacements of individual elements. The numerical models, on the other hand, by design have an idealized geometry, as well as clearly defined boundary conditions that prevent the occurrence of uncontrolled deformations of the entire system. As a second criterion for verifying the correctness of the numerical results, the convergence of representative equilibrium paths was adopted. Similarly to the experimental results, the relationship of the element's strain angle as a function of the applied load was considered. The combined graph of the equilibrium paths, obtained through experimental methods and as a result of numerical simulations, is presented below (Figure 10).

In both analyzed cases, the equilibrium paths show consistency between the graphs obtained from numerical calculations and those from experimental studies. Some irregularity observed in the experimental graphs at low levels of

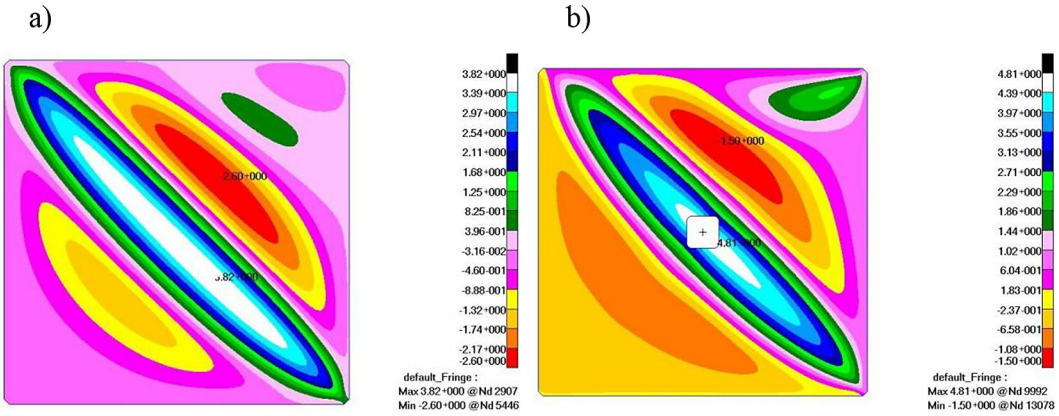

Figure 9. Distribution of displacements in the direction normal to the surface: (a) element without a cutout, (b) element with a cutout

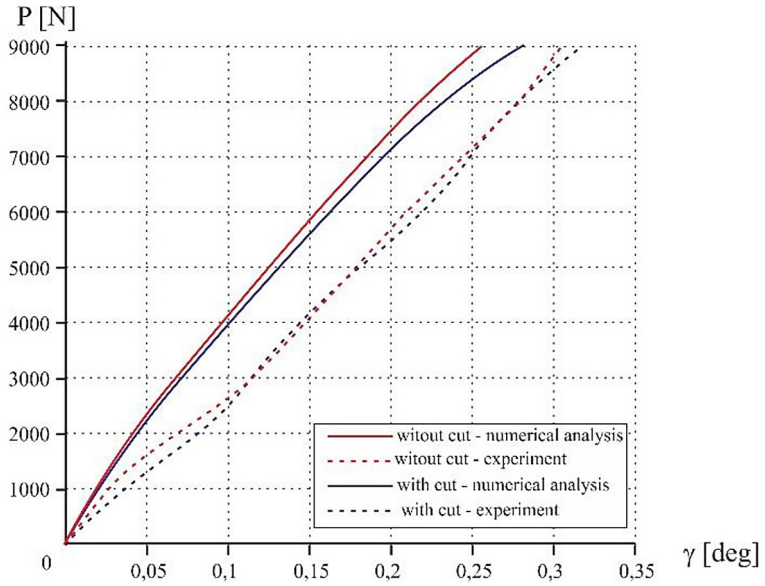

Figure 10. Equilibrium paths obtained from numerical calculations and experimental studies

applied load can be explained by the elimination of gaps in the loading system and minor displacements of the tested elements within the frames. The differences in the values of the strain angle between the computational models and the actual objects were within the range of 15% for maximum load. Larger discrepancies were observed at lower load values due to the presence of clearances and geometric imperfections in the actual components.

Considering the consistency of both the deformation shapes and the equilibrium paths, it was accepted, in accordance with the principle of solution uniqueness, that the stress distributions obtained through numerical methods are correct both qualitatively and quantitatively. Below is the presentation of the reduced stress distribution according to the Huber-Mises-Hencky hypothesis (Figure 11). By analyzing the images of the reduced stress distributions, very high values (reaching around 325 MPa) and stress gradients can be observed in the corner areas for both analyzed elements. These regions are particularly susceptible to damage due to the effects of cyclic loads. In the case of the element with a cutout, a significant concentration of stresses can also be observed in its corners. In a small area, the stresses increase from approximately 80 MPa to nearly 400 MPa. Despite its small size, the cutout has led to the emergence of a zone particularly at risk of premature fatigue failure. Given that we are dealing with thin-walled elements, it is also necessary to analyze the distributions of maximum normal stresses (Figure 12).

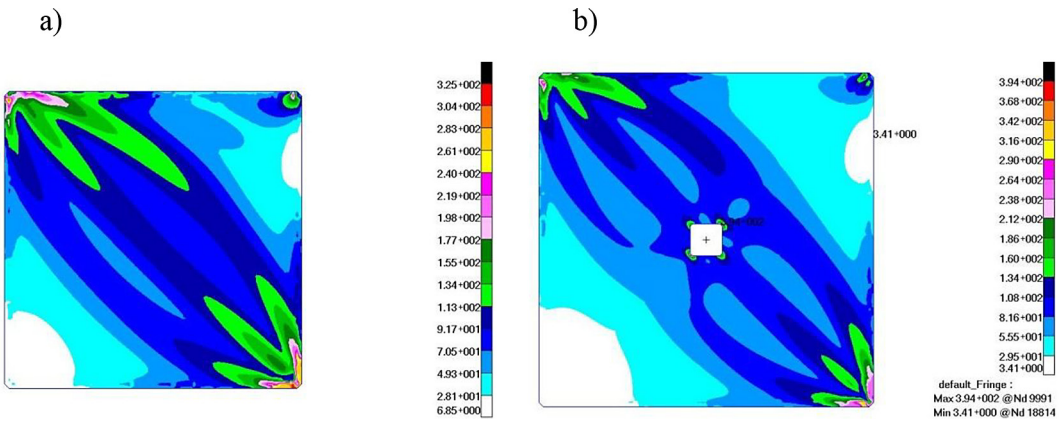

Figure 11. Distribution of stresses according to the Huber-Mises-Hencky hypothesis: (a) element without a cutout, (b) element with a cutout

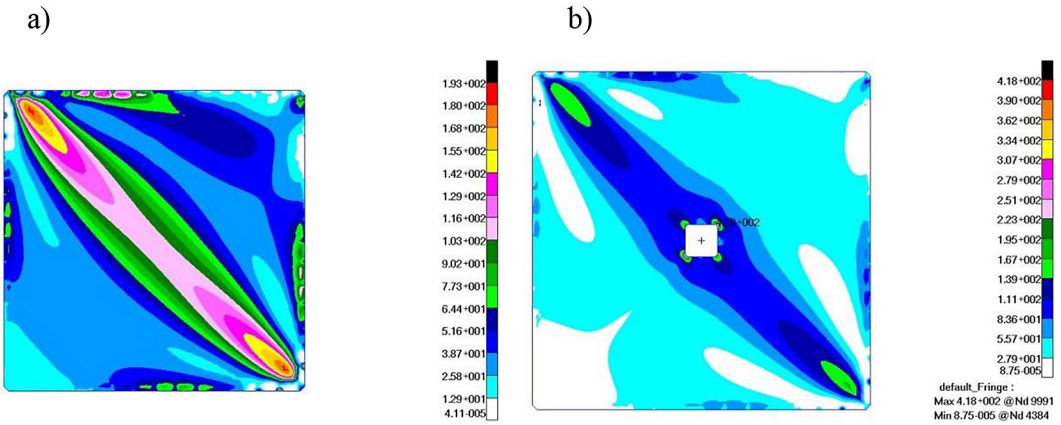

Figure 12. Distribution of principal stresses σ_1: (a) element without a cutout, (b) element with a cutout

The maximum values of principal stresses σ1 for the element without a cutout reached 193 MPa and appeared in areas directly adjacent to the corners. In the case of the element with a cutout, similar stress concentration areas can also be observed in the immediate vicinity of the corners. Additionally, in the corners of the cutout, strong stress concentrations were noted, exceeding twice the maximum values in other areas of the analyzed element, reaching 418 MPa. Therefore, early onset of fatigue damage is to be expected in this region.

CALCULATIONS AND RESEARCH OF FATIGUE STRENGHT

Results of numerical analysis of structures under static conditions, whose accuracy is additionally verified by appropriate experimental studies, are often sufficient evidence for appropriate institutions to approve the structure for operation. However, a significant majority of structural elements are subjected to varying or cyclically varying loads [21]. Such loads most often lead to premature failure of the structure (80–95% of all failure cases). Therefore, more frequently, in addition to static condition calculations, fatigue strength analysis of selected, critical areas is also performed. The load patterns occurring during long-term operation, especially in relation to aircraft structures, are random, depending on the nature of the operation and the lack of repeatability of weather conditions. The actual load spectrum, recorded during the current operation of structures with similar purposes, is subjected to statistical analysis to obtain an equivalent spectrum. Based on this, fatigue analysis and experimental testing of the prototype are carried out [22–24].

For assessing the fatigue strength of structural elements, Wohler curves based on fundamental cyclic testing for individual materials are used. Due to the high safety factors adopted, for many years, it was sufficient to primarily consider the

area corresponding to high-cycle fatigue. In this range of loading, primarily elastic deformations occur. Currently, there is an increasing use of an approach that takes into account both elastic and plastic deformations. This type of analysis is known as ε-n analysis. The criterion for failure here is the critical amplitude of plastic deformation ε_{apl} or total deformation ε_{ac} that occurs at the moment of crack initiation. Theoretical considerations and experimental studies conducted over the years have demonstrated the usefulness of this method even for metals that exhibit low elastic deformation.

Cyclic deformation curves of metals are usually presented in the σ_a – *log* ε_{apl} coordinate system. They are straight lines or approximately linear with the equation:

$$\sigma_a = k'(\varepsilon_{apl})^{n'} \quad (1)$$

where: n' – cyclic strengthening exponent, k' – fatigue strength coefficient.

For example, considering Morrow's formula [12, 21], the total deformation amplitude ε_{ac}, which consists of elastic deformation (ε_{as}) and plastic deformation (ε_{apl}), can be expressed as follows:

$$\varepsilon_{ac} = \varepsilon_{as} + \varepsilon_{apl} = \frac{\sigma_f'}{E}(2N_f)^b + \varepsilon_f'(2N_f)^c \quad (2)$$

where: σ_f' – fatigue strength coefficient, $2N_f$ – number of load cycles, b – fatigue strength exponent, E – Young's modulus, ε_f' – plasticity coefficient under variable loading, c – plasticity exponent under variable loading.

The above relationship can be interpreted as a superposition of the ε_{as} (elastic deformation) and ε_{apl} (plastic deformation) curves in the log *log* ε_a – *log*$2N_f$ coordinate system (Figure 13).

The intersection point of the lines ε_{apl} and ε_{as}, (point *t*) is referred to as the transitional point.

The information obtained from numerical calculations regarding the stress distribution in the analyzed elements allowed for the conducting of numerical simulations of fatigue strength based on the ε-n analysis model, using the MSC Fatigue software [12]. To perform the calculations, a material model corresponding to the properties of aluminum alloy 2024 [17, 18] was generated in the 'Material Management' module. The static parameters are presented in the Table 1. The fatigue parameters of the alloy are presented below (Table 2).

For the calculations, maximum normal stresses were selected as the target component of the stress state. To account for local plastic deformations, the Neuber correction was applied. [22, 25–27]. The mean stress correction of Smith–Watson–Topper

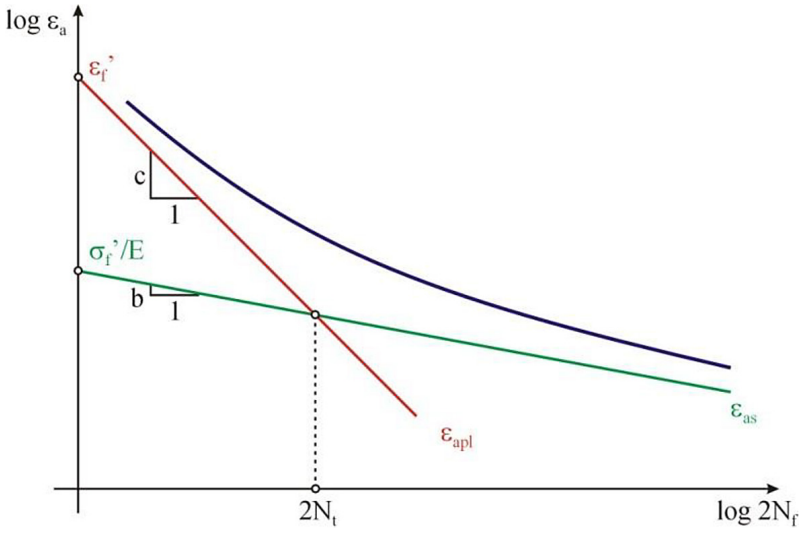

Figure 13. ε_a - ($2N_f$) graph

Table 2. Fatigue properties of Alloy 2024

σ_f'	*b*	*c*	ε_f'	*n'*	*K'*
[MPa]	[-]	[-]	[-]	[-]	[MPa]
1013,53	-0,11	-0,52	0,21	0,09	786

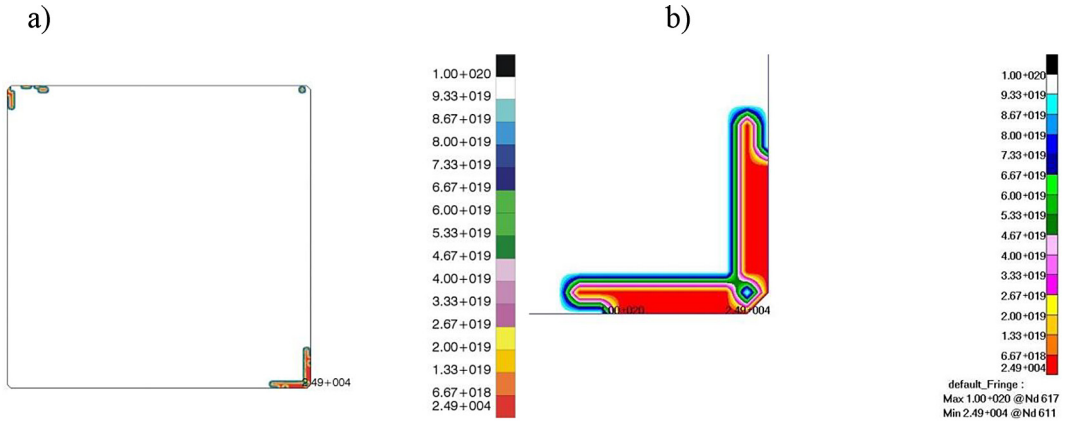

Figure 14. Colour maps illustrating the number of cycles of the element without cutout: (a) global view, (b) close-up of the critical zone

was used [12, 22, 28]. The simulation was conducted for the case of sinusoidally varying symmetrical loads. As a result of the numerical calculations, contour plots were obtained, illustrating the areas where a fatigue crack of 2 mm length is expected to occur. Below is an illustration of the critical zones, expressed in terms of the number of cycles corresponding to fatigue damage, for the element without any cutout (Figure 14).

The critical area occurs in the vicinity of the corner, along the line connecting the analyzed element with the rigid edges. The conducted calculations indicated a risk of fatigue damage after approximately 24,900 cycles of operation.

An analogous simulation was conducted for the case of the element with a cutout. The occurrence of high levels of maximum normal stresses and their strong gradients at the corners of the cutout suggested the emergence of critical zones in this area, which are significantly more susceptible to damage than the edge of the element. Colour maps depicting the fatigue strength of the element with a cutout are presented below (Figure 15).

As a result of the conducted calculations, the fatigue strength was determined to be approximately 6000 cycles. The simulations conducted revealed that introducing a cutout in the analyzed element significantly reduces its fatigue strength. Fatigue damage may occur at a dramatically lower number of cycles compared to the element without a cutout. However, numerical simulations are subject to the possibility of a series of errors. The calculations are based on stress distributions, the values of which obtained numerically may differ from the actual values. Another factor affecting the consistency of the calculation results with the durability of the actual structure is the repeatability of material parameters in production conditions. Additionally, the precision of the assembly of the analyzed elements within the complete structure is also a significant issue. These factors indicate that each structure should

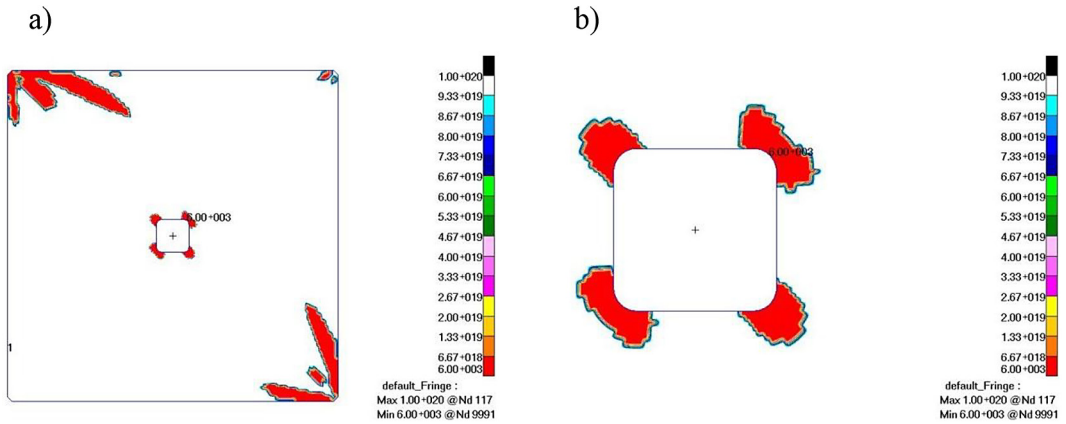

Figure 15. Colour maps illustrating the number of cycles of the element with a cutout: (a) global view, (b) close-up of the critical zone

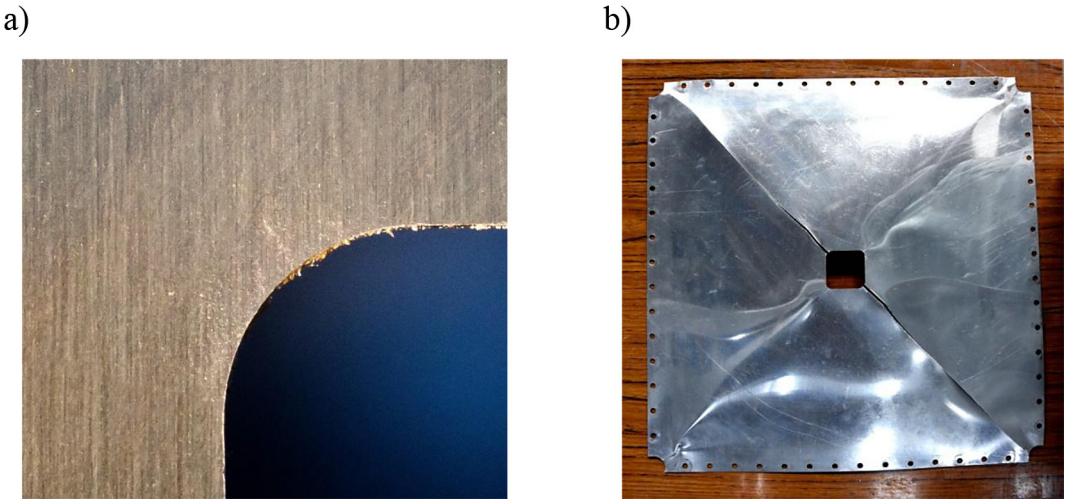

Figure 16. (a) crack of 1.4 mm in length after 5750 cycles, (b) complete failure after approximately 9000 cycles

undergo experimental fatigue testing, at least in relation to the scenario that best reflects normal operating conditions.

A simplified load spectrum with only maximum values based on a constant amplitude was used. Numerical calculations can be performed for any operational load spectrum without the need for costly experimental tests in each case. To generalize the calculations for different scenarios, one of the available cycle asymmetry correction strategies is employed. In order to verify the numerical simulations of fatigue strength, experimental tests were conducted by subjecting the element with a cutout to sinusoidally varying cyclic loads. Experiments were conducted using fully reversed load cycles with a constant force amplitude and a cycle asymmetry coefficient R= - 1, at a frequency of f = 0.05 Hz (period T = 20 seconds). The load force value and the number of cycles were recorded. Three identical elements were sequentially tested, documenting the symptoms of emerging fatigue damage (Figure 16).

In all three cases, similar results were obtained. The lengths of the fatigue cracks at various stages of cracking are summarized in the table (Table 3) and presented as a crack propagation rate graph (Figure 17). The presented graph allows for determining the critical crack length of

Table 3. Crack growth as a function of the number of cycles

Number of cycles	5750	5850	6000	6500	7000	7500	8000
Crack lenght [mm]	1.4	1.8	2.5	4.5	7.5	13	30

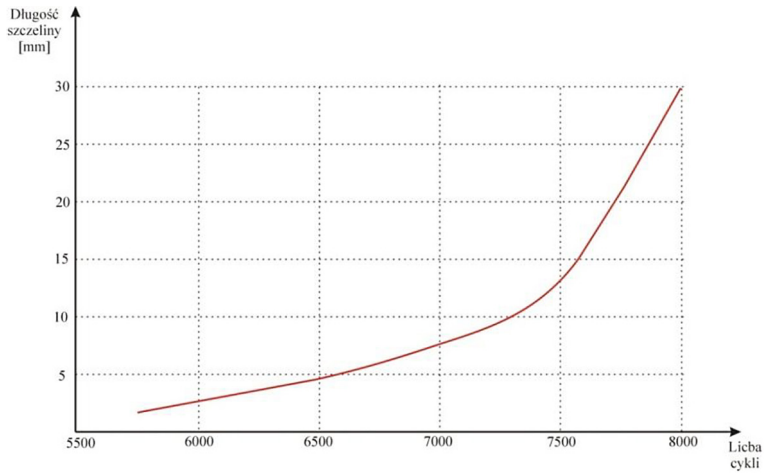

Figure 17. Crack propagation rate graph

approximately 15 mm, which appears after more than 7500 cycles. This represents an increase of approximately 25% relative to the number of cycles leading to a 2 mm fatigue failure, according to the criterion adopted in the ε-n analysis. After this period, the crack begins to grow rapidly.

CONCLUSIONS

The results presented in this study allow for drawing a series of practical conclusions. The distributions of normal displacements to the surface obtained from experimental research enabled the generation of numerical models that provide satisfactory conformity of deformation shapes under maximum load. The slight additional folds observed during experimental tests, which were not present in the numerical solution, stem from the extensive idealization of the virtual model, which is unattainable for real objects. Such imperfections do not significantly affect the overall validity of the solution. The agreement between the numerical and experimental representative equilibrium paths, which define the shape deformation angle as a function of the applied load, was also confirmed as a second criterion. Minor discrepancies in the initial loading phase, observed between the experimental and numerical curves, resulted from the elimination of play that existed in the actual loading setup and could not be replicated in the numerical models.

The obtained stress distribution results showed that in the element with a cutout, critical areas formed at the corners of the hole, where significant stress concentrations were observed. Their values were more than 21% higher than in the case of the element without a cutout.

The satisfactory agreement between the results of experimental tests and numerical calculations allowed for the conclusion that the generated computational models provide accurate stress distributions. This made it possible to conduct numerical simulations of fatigue strength. The results obtained showed a significant reduction in the resistance of the element with a cutout, by as much as four times, compared to a similar element without a cutout when subjected to variable loads.

The large number of factors influencing the emergence of symptoms of fatigue damage in a real structure, such as the repeatability of material properties, accuracy of assembly of components, etc., means that one cannot rely solely on the results of numerical calculations. Experimental fatigue tests conducted on the element weakened by a cutout showed a high level of agreement with the results obtained through numerical methods. A mere few percent discrepancy between the results of numerical simulations and those from experiments conducted on three test elements indicates that the computational model was accurately generated. Therefore, using this model, it is also possible to conduct a series of fatigue strength analyses utilizing various spectra of variable loads. The studies presented in the article were conducted for cyclic loading scenarios, simulating the maximum values to which a thin-walled component may be subjected when functioning as the covering of aerospace structures. Obtaining accurate results from numerical analysis, in comparison to the behavior of the actual structure, requires taking into account a number of factors that can affect the reduction of the component's durability. First and foremost, it is essential to correctly identify the dominant component of the stress state, obtained from static analysis and used as input data for the cyclic calculations. In the case of the thin-walled elements discussed in the paper, correct results were achieved by applying the maximum principal stresses σ_1. In the case of other types of structural elements, an appropriate available component should be used (e.g., in the case of aircraft load-bearing joints, the most advantageous is the reduced stress according to the Huber-Misses-Hencky hypothesis). Another factor is the spectrum of operational loads, which are stochastic in nature. The influence of different load levels is taken into account by introducing a replacement spectrum and selecting a correction strategy (in the MSC). Fatigue program, options include Morrow correction and Smith–Watson–Topper. Additionally, some programs allow for consideration of surface treatment, thermal and thermochemical processes, as well as the impact of a corrosive environment. Considering all these factors is a very complex task, and as a result, the results obtained through numerical calculations should be regarded as approximate values that help identify critical zones and estimate the approximate time of damage development.

The proposed methodology, combining the parallel use of nonlinear numerical analyses with appropriate experimentation, will be applied to expand the range of considered structural systems to include individual elements with geometric discontinuities as well as larger thin-walled structures.

REFERENCES

1. Debski H.: Stability problems of compressed thin-walled structures, Advances in Science and Technology-Research Journal, 2018; 12(4): 190–198.
2. Debski H., Teter A.: Numerical and experimental studies on the limit state of fibre-reinforced composite columns with a lipped channel section under quasi-static compression, Composite Structures, Published: DEC 1 2015; 133: 1–7.
3. Falkowicz K., Debski, H.: Postbuckling behaviour of laminated plates with a cut-out, Advances in Science and Technology-Research Journal, 2017; 11(1): 186–193.
4. Falkowicz K., Ferdynus M., Debski H.: Numerical analysis of compressed plates with a cut-out operating in the geometrically nonlinear range, Eksploatacja i Niezawodnosc -Maintenance and Reliability, 2015; 17(2): 222–227.
5. Wysmulski P., Debski H., Rozylo P., Falkowicz K.: A study of stability and post-critical behaviour of thin-walled composite profiles under compression; Eksploatacja i Niezawodnosc-Maintenance and Reliability, 2016; 18(4): 632–637.
6. Kopecki T.: Numerical-experimental analysis of the post-buckling state of a multi-segment and multi-member thin-walled structure subjected to torsion; Journal of Theoretical and Applied Mechanics, 2011; 49(1): 227–242.
7. Kopecki T.: Numerical and experimental analysis of post-critical deformation states in a tensioned plate weakened by a crack; Journal Of Theoretical and Applied Mechanics, 2010; 48(1): 45–70.
8. Kopecki T., Mazurek P.: Determination of stress distribution patterns in post-criticaldeformation states of thin-walled skins subjected to operating loads; Eksploatacja i Niezawodnosc - Maintenance and Reliability, 2014; 16(4): 608–615.
9. Kopecki T., Święch Ł.: Experimental and numerical analysis of post-buckling deformation states of integrally stiffened thin-walled components of load-bearing aircraft structures; Journal of Theoretical and Applied Mechanics, 2014; 52(4): 905–915.
10. Kopecki T., Święch Ł.: Experimental-numerical analysis of a flat plate subjected to shearing and manufactured by incremental techniques, Advances in Science and Technology-Research Journal, 2023; 17(4): 179–188.
11. Bathe K.J.: Finite element procedures in engineering analysis, Prentice-Hall, Englewood Cliffs 1982.
12. MSC Software: MSC Fatigue 2017, User's Guide, MSC.Software Corporation, 2016.
13. MSC Software: MSC MARC 2017, User's Guide, MSC.Software Corporation, 2016.
14. Fe-safe fatigue theory reference manual, Dassault Systèmes, 2019.
15. DesignLife Theory Guide (nCode 9), HBM Prenscia, 2014.
16. The Fatigue Module of ANSYS Mechanical, ANSYS Inc., 2015.
17. Benachour N., Hadjoui A., Benachour M., Benguediab M.: Stress ratio and notch effect on fatigue crack initiation and propagation in 2024 al-alloy. International Journal of Mechanical and Mechatronics Engineering 2011; 5(7): 1384–1387.
18. Khan S.S.: Low cycle lifetime assessment of Al 2024 alloys, Helmholtz-Zentrum Geesthacht, Zentrum für Material- und Küstenforschung GmbH, Geesthacht 2012.
19. Felippa C.A.: Advanced finite element methods, (ASEN 5367) Dept. of Aerospace Eng. Sci. Bouilder, Colorado 2006.
20. Felippa C.A.: Nonlinear finite element methods, (ASEN 5107) Dept. of Aerospace Eng. Sci. Bouilder, Colorado 2006.
21. Kocańda S., Szala J.: Podstawy obliczeń zmęczeniowych, Wydawnictwo Naukowe PWN, Warszawa 1997.
22. Schijve J.: Fatigue of Structures and Materials, Springer Science+Business Media, B.V. 2009.
23. Leski A.: Ocena trwałości struktury nośnej statków powietrznych na podstawie badań doświadczalnych i analiz numerycznych. ITWL, Warszawa 2012.
24. Gruszecki H., Chodur J., Pietruszka J.: Badania zmęczeniowe metalowej struktury lotniczej samolotu kategorii „Commuter, II Konferencja „Zmęczenie konstrukcji lotniczych", Warszawa, 15–16 stycznia 2009.
25. Neuber H.: Theory of stress concentration for shear-strained prismatical bodies with arbitrary nonlinear stress-strain law, ASME Journal of Applied Mechanics 28, 1961.
26. Kilambi S.: Numerical evaluation of the original Neuber's Rule for pure out-of-plane shear loading, The Journal of Strain Analysis for Engineering Design, August 2013.
27. Samuelsson L.: Fatigue Analysis: The Super-Neuber Technique for Correction of Linear Elastic Fe Results, 26th International Congress Of The Aeronautical Sciences, Anchorage, 2008.
28. Ince A, Glinka G.: A modification of Morrow and Smith–Watson–Topper mean stress correction models, Fatigue & Fracture of Engineering Materials & Structures 2001; 34: 854–867.